Nonadiabatic and anharmonic effects in high-pressure H₃S and D₃S superconductors

Shashi B. Mishra^{1,*} and Elena R. Margine^{1,†}

¹Department of Physics, Applied Physics and Astronomy,
Binghamton University-SUNY, Binghamton, New York 13902, USA

(Dated: October 31, 2025)

Superconductivity in compressed H_3S arises from the interplay between high-frequency phonons and a pronounced van Hove singularity near the Fermi level. Using first-principles calculations, we investigate the superconducting properties of H_3S and D_3S at 160 and 200 GPa, explicitly incorporating anharmonic lattice dynamics and first-order vertex corrections to electron-phonon (e–ph) interactions, thereby going beyond the Migdal approximation underlying conventional Migdal-Eliashberg theory. We find that both anharmonicity and nonadiabatic vertex corrections suppress the effective e-ph coupling and reduce the superconducting critical temperature (T_c). Calculations performed within the energy-dependent full-bandwidth Eliashberg formalism, including both anharmonic and vertex effects, yield T_c values in close agreement with experimental measurements for D_3S at both pressures and for H_3S at 200 GPa.

Keywords: Electron-phonon coupling, vertex effect, anharmonicity, superconductivity, isotope effect

I. INTRODUCTION

The quest for room-temperature superconductivity has accelerated after the discovery of high critical temperatures (T_c) in H₃S under extreme pressure [1]. Subsequent studies have revealed several other hydrogenrich compounds as promising candidates for near-room-temperature superconductivity [2–6], and more recently, evidence of room-temperature superconductivity has been reported in the La-Sc-H system [7]. These advances have been enabled by major developments in high-pressure synthesis and characterization techniques, pioneered largely by M. Eremets and collaborators [3, 4, 8, 9]. In parallel, ab initio predictions have guided experimental efforts by identifying candidate structures and elucidating superconducting properties in hydrogen-rich materials [10–20].

The theoretical basis of hydride superconductivity can be traced back to Ashcroft's hypothesis [21] that metallic hydrogen could achieve high- $T_{\rm c}$ through conventional electron-phonon (e-ph) coupling [22]. Recognizing the experimental challenges posed by the high pressures required to metallize pure hydrogen, Ashcroft subsequently proposed that hydrogen-rich materials, in which hydrogen atoms experience chemical precompression from heavier elements, could become metallic and superconducting under experimentally accessible conditions, broadening the search to hydrogen-containing alloys and compounds [23]. A defining feature of these hydrides is the combination of high vibrational frequencies and strong e-ph coupling, which underpins their high- $T_{\rm c}$ behavior.

Within the hydride family, H₃S has emerged as the prototypical system, in which superconductivity is driven by two key ingredients: the exceptionally high-frequency

vibrations of hydrogen atoms (maximum phonon frequency, $\omega_{\rm ph} \approx 200-250$ meV) and a pronounced van Hove singularity (vHs) located near the Fermi level. The narrow width of the vHs leads to a relatively small Fermi velocity, $(2.1-3.7)\times10^5$ m/s [24], and hence a low Fermi energy scale ($\varepsilon_{\rm F} \approx 40-50$ meV [25]). Together with the large phonon frequencies, this results in a high adiabatic ratio, $\eta = \omega_{\rm ph}/\varepsilon_{\rm F}$, which challenges the validity of Migdal's approximation [26, 27] and necessitates the inclusion of vertex corrections for an accurate theoretical description of the e-ph interaction [28, 29]. The light mass of hydrogen further amplifies anharmonic lattice vibrations, which not only stabilize the high-pressure structure [30] but also strongly renormalize the phonon spectrum and e-ph coupling strength [12, 28, 29].

The interplay between anharmonic and nonadiabatic effects becomes particularly critical when comparing theoretical predictions with experimental results. Experimental tunneling and resistivity measurements have reported superconducting gaps and transition temperatures in samples near 150–161 GPa range [9], whereas most theoretical studies have focused on higher pressures (200-250 GPa), often neglecting anharmonic contributions. In our recent work at 200 GPa [29], we demonstrated that accounting for both vertex corrections and quantum anharmonic effects significantly modifies the eph coupling and lowers the predicted T_c , bringing theoretical predictions into close agreement with experimental observations. These findings emphasize the importance of systematic ab initio investigations that incorporate anharmonicity and vertex corrections to fully capture the pressure-dependent superconductivity of H₃S and its isotopic counterparts.

Here, we extend our previous work [29] to perform a comparative analysis of H₃S and D₃S at 160 and 200 GPa, examining how e-ph coupling, vertex corrections, and anharmonic phonon renormalization evolve with pressure. We find that anharmonic effects are essential for maintaining structural stability at 160 GPa, in

^{*} mshashi125@gmail.com

[†] rmargine@binghamton.edu

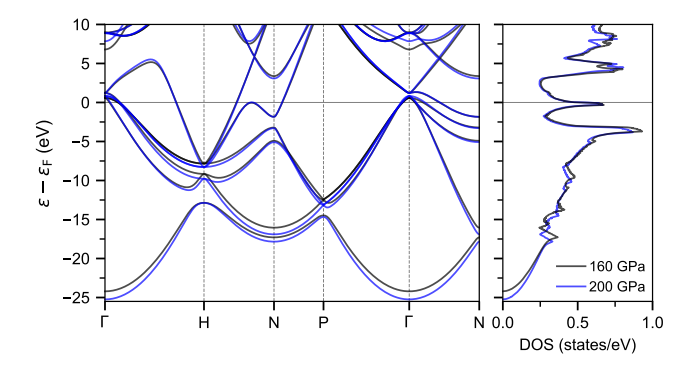


FIG. 1. Electronic band structure and density of states (DOS) of H_3S at 160 GPa (blue line) and 200 GPa (black line).

agreement with a previous study [30]. In terms of superconducting properties, both H_3S and D_3S exhibit a similar pressure dependence, with the e-ph coupling strength λ decreasing slightly as pressure increases, while the e-ph vertex correction contribution λ^V nearly doubles, leading to a reduction in the superconducting transition temperature T_c .

II. RESULTS AND DISCUSSION

 H_3S adopts the body-centered cubic $Im\bar{3}m$ phase under high pressure [8, 31], which remains experimentally stable over a broad pressure range (150–300 GPa). The superconducting $T_{\rm c}$ reaches its maximum near 150-160 GPa and gradually decreases with further compression [1, 32]. Our ab initio calculations yield optimized lattice constants of 3.049 Å at 160 GPa and 2.986 Å at 200 GPa, in good agreement with previous theoretical [10, 12] and experimental [1] reports. The electronic density of states (DOS) at the Fermi level ($\varepsilon_{\rm F}$) remains high at both pressures, characterized by a sharp vHs peak near $\varepsilon_{\rm F}$ (see Figure 1). With the increase in pressure, the DOS at $\varepsilon_{\rm F}$ remains virtually unchanged, while the free-electron-like band edge shifts to lower energies, reflecting a modest broadening of the electronic bandwidth.

At 160 GPa, the harmonic phonon dispersion of H_3S shows imaginary phonon modes around the Γ -point, indicating a saddle point on the Born-Oppenheimer potential energy surface [30] (Figure 2). To account for quantum zero-point motion and anharmonic effects, we employed the anharmonic special displacement method (A-SDM) implemented in the ZG module of EPW [33, 34]. With anharmonicity included, all phonon modes become real, confirming the dynamical stability of the $Im\bar{3}m$ phase at 160 GPa, consistent with previous work [30]. The anharmonic spectrum further reveals a noticeable hardening of the high-frequency H-derived modes, which shift upward by approximately 22 meV. For D_3S , the $Im\bar{3}m$ phase is likewise stabilized once anharmonic effects are

considered, but the corresponding high-phonon frequencies shift by only about 11 meV due to the larger atomic mass of deuterium. The strongest renormalization occurs for the H-S bond-stretching vibrations, in which hydrogen atoms move toward neighboring sulfur atoms. This pronounced anharmonicity originates from the shallow energy landscape near the second-order quantum phase transition between the $R\bar{3}m$ and $Im\bar{3}m$ phases [30].

At 200 GPa, the harmonic dispersion are positive throughout the Brillouin zone, indicating the enhanced lattice rigidity and dynamical stability of the $Im\bar{3}m$ phase even without anharmonic corrections (Figure 3). In H₃S, a small gap separates low-frequency sulfurderived from high-frequency hydrogen-derived branches around 75 meV, and the acoustic modes display the typical linear dispersion near the Γ -point. Including anharmonic effects further hardens the H-derived modes by about 25 meV, while D₃S shows a smaller shift of roughly 14 meV. Comparison of the 160 and 200 GPa results demonstrates how pressure and isotope substitution tune the phonon spectrum, setting the stage for corresponding changes in the e-ph coupling that ultimately govern the superconducting behavior of H₃S and D₃S.

To analyze the e-ph interaction, we compute the isotropic Eliashberg spectral function $\alpha^2 F(\omega)$ and the cumulative coupling strength $\lambda(\omega)$ for H₃S and D₃S (Figures 2 and 3). At 160 GPa, the H₃S Eliashberg spectral function displays a small peak in the acoustic region (below 75 meV), contributing about 30% of the total e-ph coupling, while the remainder comes from the high-frequency H-derived modes, resulting in a total λ that saturates at 1.88. The vertex-corrected spectrum $\alpha^2 F(\omega, \omega')$ is also concentrated at high phonon energies above 170 meV, yielding an integrated vertex coupling $\lambda^{\rm V} = 0.42$. D₃S at 160 GPa exhibits the same dependence but with isotope-shifted frequencies. The main peak in $\alpha^2 F(\omega)$ is lowered in energy relative to H₃S, while $\lambda(\omega)$ rises to a similar total value, $\lambda = 1.94$. Vertex contributions remain concentrated at higher phonon energies and integrate to $\lambda^{V} = 0.46$.

Although harmonic phonons are dynamically stable at 200 GPa, anharmonicity significantly renormalizes the hydrogen-derived modes, redistributing $\alpha^2 F(\omega)$, particularly above 50 meV. As a result, the integrated e-ph coupling λ drops by about 25%, from 2.29 to 1.72 [12, 29]. The reduction is even more pronounced for the vertexcorrected spectrum $\alpha^2 F(\omega, \omega')$, where anharmonicity suppresses λ^{V} by nearly 60%, from 1.78 to 0.71. D₃S follows the same trend, albeit with slightly smaller shifts consistent with its heavier isotope mass, with λ decreasing from 2.29 to 1.78 and $\lambda^{\rm V}$ from 1.78 to 0.79. Comparing the anharmonic results at the two pressures, λ decreases only marginally, while λ^{V} nearly doubles as pressure rises from 160 to 200 GPa for both H₃S and D₃S, as summarized in Table I. This increase in λ^{V} correlates with a moderate enhancement of the adiabatic parameter η , which rises from approximately 4.5-5.6 at 160 GPa to 5.0-6.2 at 200 GPa. The enhancement originates pri-

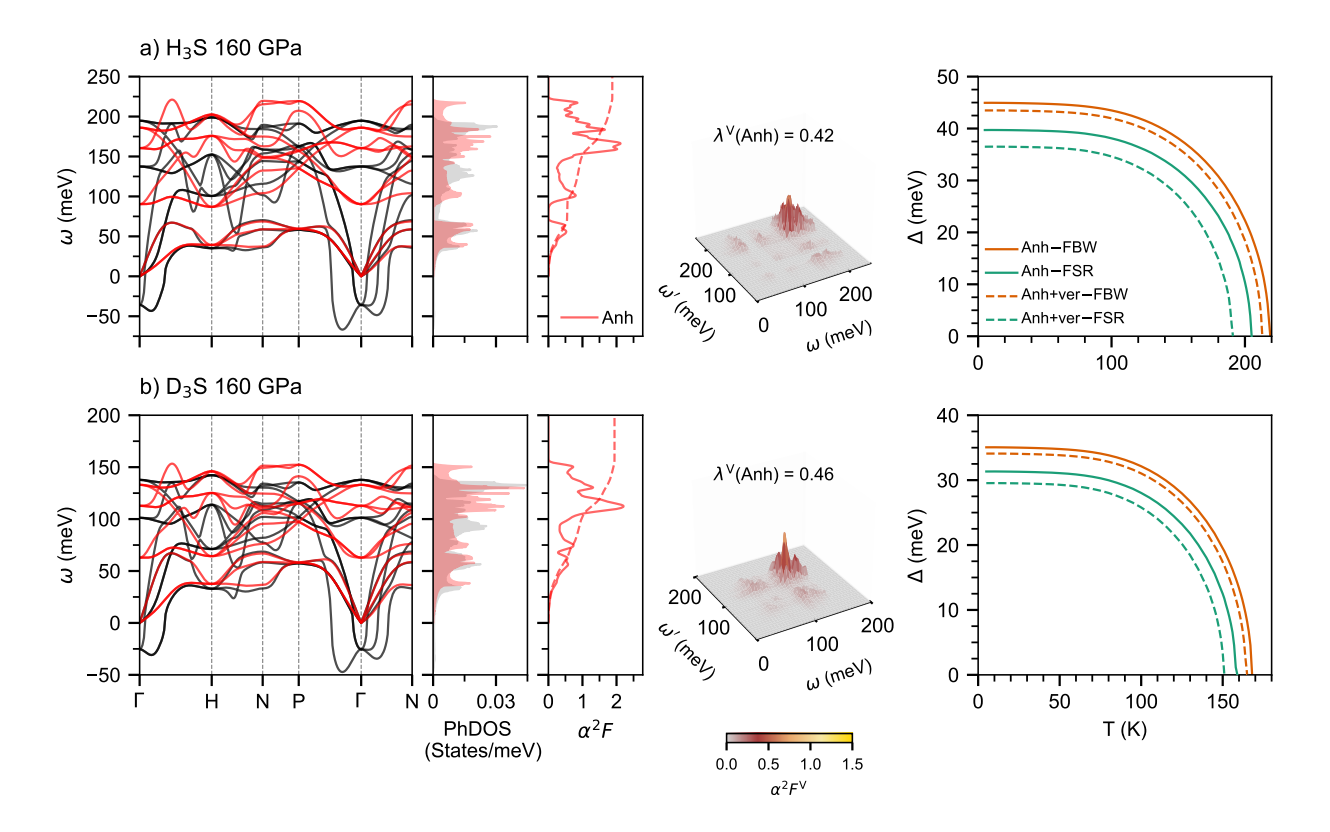


FIG. 2. a) Phonon dispersion and phonon density of states (PhDOS) of H_3S at 160 GPa calculated within the harmonic (black) and anharmonic (red) approximations. The Eliashberg spectral function $\alpha^2 F(\omega)$ (solid lines) and its cumulative e-ph coupling $\lambda(\omega)$ (dashed lines) are shown along with the spectral function from vertex corrections $\alpha^2 F^V(\omega, \omega')$ and its integrated coupling strength λ^V . The isotropic superconducting gap $\Delta(T)$ is computed using four approaches with anharmonic phonons and an effective Coulomb pseudopotential $\mu_E^* = 0.16$: FBW (orange), FSR (teal-green), vertex-corrected FBW (dashed orange), and vertex-corrected FSR (dashed teal-green). b) Corresponding results for D_3S at 160 GPa.

marily from the anharmonic hardening of $\omega_{\rm ph}$ from about 225 to 250 meV, while the Fermi energy remains nearly constant. Upon isotopic substitution, η in D₃S also increases slightly, from about 3.0-3.8 to 3.3-3.8 over the same pressure range.

Building on the phonon and e-ph coupling analysis, we examine the superconducting properties of H_3S and D_3S . To this end, we solve the isotropic Eliashberg equations for the superconducting gap $\Delta(T)$ using both the Fermisurface-restricted (FSR) and full-bandwidth (FBW) approaches [19, 29, 34]. In the FSR approximation, the density of states is treated as constant near $\varepsilon_{\rm F}$, whereas the FBW formalism explicitly retains its energy dependence. All calculations include anharmonic phonons and nonadiabatic vertex corrections, and use a Coulomb pseudopotential of $\mu_{\rm E}^* = 0.16$. The isotropic treatment is justified by prior superconductivity calculations using the anisotropic Eliashberg formalism, which showed that H₃S remains a single-gap, weakly anisotropic superconductor in the 180–200 GPa pressure range [19, 35]. This conclusion is further supported by recent tunneling spectroscopy and upper critical field measurements, which indicate that at 158 GPa, H₃S exhibits a nearly isotropic superconducting gap characteristic of strongcoupling conventional superconductivity [9].

Figures 2 and 3 show the temperature dependence of the superconducting gap $\Delta(T)$, where the critical temperature T_c is defined as the point at which Δ vanishes. A summary of the computed transition temperatures and their comparison with experimental and previous theoretical results is provided in Figure 4 and Table I. For H_3S , adiabatic FSR calculations yield $T_c =$ 205 K, close to the upper limit of the experimental range (184–203 K) reported for samples measured between 150-161 GPa [1, 8, 9, 32, 36, 37]. At this pressure, the FBW estimate is slightly higher but remains comparable to earlier theoretical predictions based on the FSR approach [30]. Including vertex corrections reduces T_c , giving 191 K for ver-FSR and 213 K for ver-FBW, with the former lying near the middle of the experimental range. Substituting hydrogen with deuterium lowers the critical temperature by approximately 40-50 K, depending on the computational method employed. For D₃S, the ver-FBW result ($T_c = 165 \text{ K}$) shows excellent agreement with experimental measurements of 163-166 K obtained between 150-161 GPa in Ref. [32]. The reduction in $T_{\rm c}$ for D₃S is directly linked to the lower characteristic phonon frequency ω_{\log} . While the e-ph coupling is only

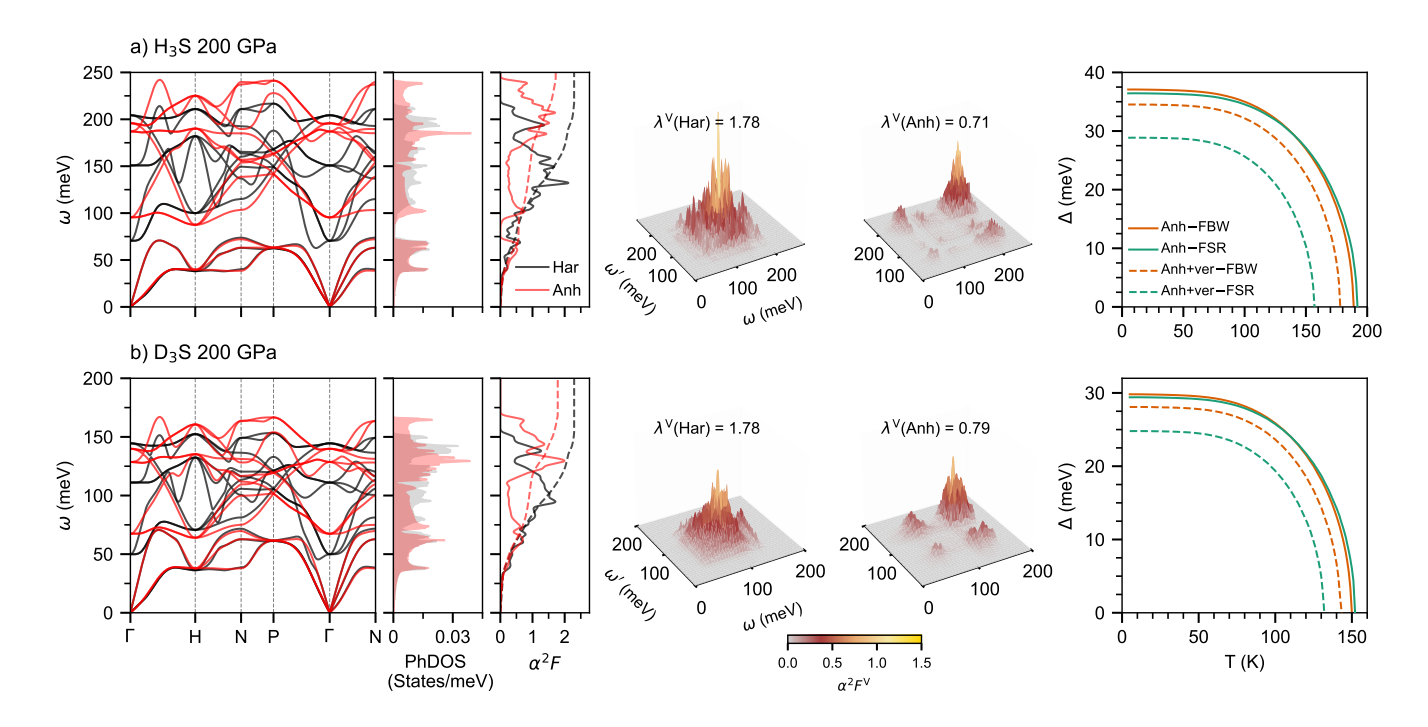


FIG. 3. a) Phonon dispersion and phonon density of states (PhDOS) of H_3S at 200 GPa calculated within the harmonic (black) and anharmonic (red) approximations. The Eliashberg spectral function $\alpha^2 F(\omega)$ (solid lines) and its cumulative e-ph coupling $\lambda(\omega)$ (dashed lines) are shown along with the spectral function from vertex corrections $\alpha^2 F^V(\omega, \omega')$ and its integrated coupling strength λ^V . The isotropic superconducting gap $\Delta(T)$ is computed using four approaches with anharmonic phonons and an effective Coulomb pseudopotential $\mu_E^* = 0.16$: FBW (orange), FSR (teal-green), vertex-corrected FBW (dashed orange), and vertex-corrected FSR (dashed teal-green). b) Corresponding results for D_3S at 200 GPa.

weakly isotope dependent, the characteristic phonon frequency scales approximately with the inverse square root of the atomic mass, decreasing by 25 meV in D_3S relative to H_3S , as shown in Table I. At 200 GPa, the verFBW approach yields 178 K for H_3S and 143 K for D_3S . These values again fall within the corresponding experimental ranges of 175–185 K for measurements between 192–208 GPa in H_3S [1, 8, 38] and 142–146 K for measurements between 195–205 GPa in D_3S [1].

At 200 GPa, we also compute the superconducting gap using harmonic phonons for both isotopes (see Supplementary Figure S1 and Table I). In this case, the larger e-ph coupling and comparable logarithmic phonon frequency lead to a systematic overestimation of $T_{\rm c}$ relative to experiment. Even after including vertex corrections, the harmonic FBW and FSR approaches yield values well above the measured ranges. Among all methods tested, the ver-FBW scheme with anharmonic phonons provides the most consistent description for both H_3S and D_3S , demonstrating that an accurate treatment of phonon anharmonicity, the energy-dependent DOS near Fermi level, and e-ph vertex corrections is essential for a realistic description of superconductivity in hydrogenrich compounds.

Several key trends emerge from the data in Table I. First, D₃S exhibits weaker vertex effects than H₃S, reflecting its lower maximum phonon frequency and corre-

spondingly smaller $\alpha^{\rm ver}$. Second, when both vertex corrections and anharmonic effects are included, the FSR-derived $T_{\rm c}$ values remain systematically below those from the FBW approach. As discussed in Ref. [29], this difference arises because, in the ver-FSR formulation, the Eliashberg equations are solved using only the value of the DOS at the Fermi level. In $\rm H_3S$ and $\rm D_3S$, the presence of the vHs near $\varepsilon_{\rm F}$ enhances this local DOS contribution, whereas the ver-FBW framework captures the full energy dependence of the DOS, yielding a more accurate and physically complete description.

Finally, we examine the isotope coefficient, defined as $\alpha = -\ln(T_c^{\mathrm{D_3S}} - T_c^{\mathrm{H_3S}})/\ln(M^{\mathrm{D_3S}} - M^{\mathrm{H_3S}})$, where $M^{\mathrm{D_3S}}$ and $M^{\mathrm{H_3S}}$ are the corresponding isotopic masses. The dependence of α on the phonon treatment and computational approach used to evaluate the superconducting properties is summarized in Table S1 of the Supplemental Material [39]. At 160 GPa, our calculations yield $\alpha = 0.34-0.38$, slightly above the experimental range of 0.22-0.34 [1, 32]. At 200 GPa, α decreases to 0.25-0.34, in good agreement with the measured values of 0.23-0.38. In contrast, harmonic phonon calculations predict substantially larger α values (0.34-0.45). Errea et al. [12, 30] reported a similar trend, obtaining $\alpha = 0.42$ at 160 GPa and 0.37-0.45 for anharmonic and harmonic phonons at 200 GPa. Other studies [40, 41] also found α values between 0.35 and 0.47, although direct compari-

TABLE I. Electron-phonon coupling strength (λ) , vertex-corrected e-ph coupling strength $(\lambda^{\rm V})$, logarithmic average phonon frequency $(\omega_{\rm log})$, and superconducting critical temperature $(T_{\rm c})$ obtained from the FSR and FBW approaches, with and without vertex corrections for H₃S and D₃S, incorporating anharmonic phonons at 160 GPa and both harmonic and anharmonic phonons at 200 GPa. All superconductivity calculations employ a Coulomb pseudopotential $\mu_{\rm E}^*$ =0.16. Experimental $T_{\rm c}$ values are taken from measurements in the 150–161 GPa [1, 8, 9, 32, 36–38] and 192–208 GPa pressure ranges for H₃S, and 150–165 GPa and 195–205 GPa pressure ranges for D₃S [1, 8, 32]. Theoretical FSR results from Refs. [12, 30] are included for comparison. All $T_{\rm c}$ values are given in K.

Element	Pressure	Phonons	λ	$\lambda^{ m V}$	ω_{log}	W/o vertex correction		With vertex correction		$T_{\mathrm{c}}^{\mathrm{Exp}}$	$T_{\mathrm{c}}^{\mathrm{FSR}}$
	(GPa)				(meV)	$T_c^{\rm FSR}$	T_c^{FBW}	$T_c^{\text{ver-FSR}}$	$T_c^{\text{ver-FBW}}$		[12,29]
$_{ m H_3S}$	160	Anh	1.88	0.42	107	205	219	191	213	184-203	213-215
	200	Har	2.29	1.78	107	246	235	198	222	175-185	250
		Anh	1.72	0.71	110	192	189	157	178	110-100	194 - 198
D_3S	160	Anh	1.94	0.46	82	159	168	151	165	163 - 166	160
	200	Har	2.29	1.78	79	180	174	157	166	142-146	183
		Anh	1.78	0.79	85	152	150	132	143	112 110	152

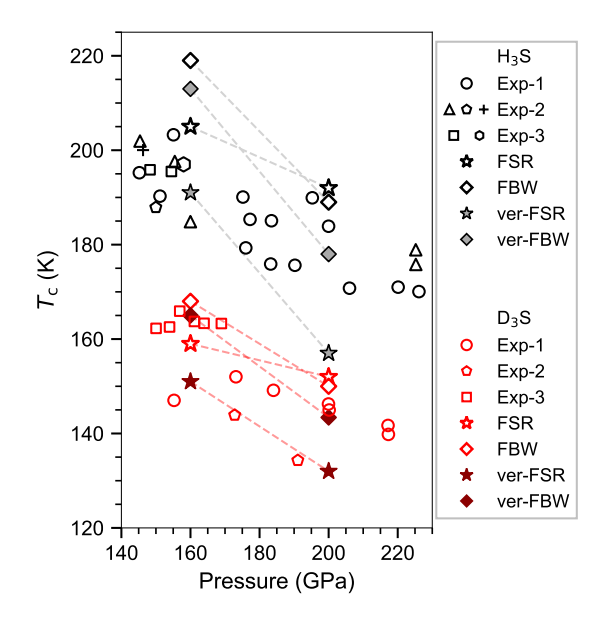


FIG. 4. Superconducting critical temperatures (T_c) calculated with anharmonic phonons for H_3S and D_3S at 160 and 200 GPa using four approaches: FSR (open star), FBW (open diamond), ver-FSR (filled star), and ver-FBW (filled diamond). Experimental data extracted from the literature are shown for comparison and labeled as Exp-1 [1], Exp-2 [8, 36–38], and Exp-3 [9, 32]. Black symbols represent H_3S and red symbols represent D_3S .

son is complicated by differences in the adopted Coulomb pseudopotential μ^* used to reproduce the experimental $T_{\rm c}.$

This ratio exceeds the experimentally observed $\Delta(0)$ values of 29–31.5 meV for samples measured around 151–161 GPa, corresponding to a BCS ratio of 3.55 [9]. Although the experimental value suggests a weak-coupling limit [22], H₃S is in fact a strong-coupling super-

conductor. The discrepancy might be attributed to uncertainties or differences in the experimental extraction and fitting procedures for the superconducting gap methods used to interpret tunneling spectra, as well as the limitations of our theoretical calculations. Further theoretical calculations using different exchange-correlation functionals [42], and systematic experimental studies over a wider pressure range might be useful.

III. CONCLUSION

We investigated the influence of phonon anharmonicity and first-order e-ph vertex corrections on superconductivity in H₃S and D₃S at 160 and 200 GPa by solving the Eliashberg equations using both the FSR (constant DOS) and FBW (energy-dependent DOS) formalisms. Anharmonicity serves two key roles: it stabilizes the $Im\bar{3}m$ phase at 160 GPa and hardens the high-frequency hydrogen-derived modes, which lowers the e-ph coupling strength and suppresses $T_{\rm c}$. With increasing pressure, the conventional e-ph coupling λ decreases slightly, while the vertex-corrected coupling λ^{V} increases, indicating that nonadiabatic effects become more pronounced. The FBW approach including both anharmonic phonons and vertex effects yields $T_{\rm c}$ values in close agreement with experimental measurements for D₃S at both pressures and for H₃S at 200 GPa. We find that the lower phonon frequencies in D₃S weaken the vertex contribution and reduce T_c , consistent with a phonon-mediated pairing mechanism. These results show that accurate modeling of superconductivity in hydrogen-rich materials under extreme compression requires the combined treatment of anharmonic lattice dynamics, nonadiabatic corrections, and an energy-dependent electronic structure.

IV. COMPUTATIONAL METHODS

We performed density-functional theory (DFT) calculations using Quantum ESPRESSO [43] with optimized norm-conserving Vanderbilt (ONCV) pseudopotentials [44] generated with Perdew-Burke-Ernzerhof functional [45]. We used a plane-wave cutoff of 60 Ry, a Methfessel-Paxton smearing [46] value of 0.01 Ry, and a Γ -centered k-grid of $24 \times 24 \times 24$ to describe the electronic structure. The lattice parameters and atomic positions were relaxed until the total energy was converged within 10^{-6} Ry and the maximum force on each atom was less than 10^{-4} Ry/Å. The dynamical matrices and the linear variation of the self-consistent potential were calculated within density-functional perturbation theory [47] on a $4 \times 4 \times 4$ g-mesh. For the anharmonic calculations, we performed static DFT computations on a $12 \times 12 \times 12 \times 12$ grid, and obtained the interatomic force constants from a $4 \times 4 \times 4$ supercell with a finite displacement of 0.01 Å. All calculations were carried out at 0 K. In our previous study we showed that the anharmonic phonon dispersion at 200 GPa remains nearly unchanged even at 200 K [29].

For the e-ph interactions and superconducting properties, we employed the EPW code [19, 34, 48–50]. The electronic wavefunctions required for the Wannier inter-

polation [51–53] were obtained on a uniform Γ -centered $8\times8\times8$ k-grid using ten atom-centered orbitals, with s orbital for the H atom and $s, p, d_{xy}, d_{xz}, d_{yz}$ orbitals for the S atom. The e-ph matrix elements were then computed on uniform $48 \times 48 \times 48$ k- and $24 \times 24 \times 24$ q-point grids, with an energy window of ± 0.2 eV around the Fermi level. The electronic and phononic Dirac delta functions were replaced by Gaussians broadenings of 50 meV and 2.5 meV, respectively. The isotropic Eliashberg equations were solved on the imaginary Matsubara frequency axis using a frequency cutoff of 2.5 eV. For the convergence of the energy window in FBW calculations, the DOS was evaluated using a Fermi window of 1 eV. To capture the isotope effect, the same computational protocol was applied to D₃S by substituting the hydrogen mass with that of deuterium.

ACKNOWLEDGMENTS

This research was supported by the National Science Foundation (NSF) under Award No. DMR-2035518. Computational resources were provided by the Texas Advanced Computing Center (TACC) at The University of Texas at Austin through allocation TG-DMR180071 on the Stampede3 system, supported by NSF Award OAC-2311628.

- A. P. Drozdov, M. I. Eremets, I. A. Troyan, V. Ksenofontov, and S. I. Shylin, Conventional superconductivity at 203 kelvin at high pressures in the sulfur hydride system, Nature 525, 73 (2015).
- [2] M. Somayazulu, M. Ahart, A. K. Mishra, Z. M. Geballe, M. Baldini, Y. Meng, V. V. Struzhkin, and R. J. Hemley, Evidence for Superconductivity above 260 K in Lanthanum Superhydride at Megabar Pressures, Phys. Rev. Lett. 122, 027001 (2019).
- [3] A. P. Drozdov, P. P. Kong, S. P. Minkov, V. S. and Besedin, M. A. Kuzovnikov, S. Mozaffari, L. Balicas, F. F. Balakirev, D. E. Graf, V. B. Prakapenka, E. Greenberg, D. A. Knyazev, M. Tkacz, and M. I. Eremets, Superconductivity at 250 K in lanthanum hydride under high pressures, Nature 569, 528 (2019).
- [4] P. Kong, V. S. Minkov, M. A. Kuzovnikov, A. P. Drozdov, S. P. Besedin, S. Mozaffari, L. Balicas, F. F. Balakirev, V. B. Prakapenka, S. Chariton, et al., Superconductivity up to 243 K in the yttrium-hydrogen system under high pressure, Nat. comm. 12, 5075 (2021).
- [5] I. A. Troyan, D. V. Semenok, A. G. Kvashnin, A. V. Sadakov, O. A. Sobolevskiy, V. M. Pudalov, A. G. Ivanova, V. B. Prakapenka, E. Greenberg, A. G. Gavriliuk, I. S. Lyubutin, V. V. Struzhkin, A. Bergara, I. Errea, R. Bianco, M. Calandra, F. Mauri, L. Monacelli, R. Akashi, and A. R. Oganov, Anomalous High-Temperature Superconductivity in YH6, Adv. Mater. 33, 2006832 (2021).
- [6] L. Ma, K. Wang, Y. Xie, X. Yang, Y. Wang, M. Zhou,

- H. Liu, X. Yu, Y. Zhao, H. Wang, G. Liu, and Y. Ma, High-Temperature Superconducting Phase in Clathrate Calcium Hydride CaH₆ up to 215 K at a Pressure of 172 GPa, Phys. Rev. Lett. **128**, 167001 (2022).
- [7] Y. Song, C. Ma, H. Wang, M. Zhou, Y. Qi, W. Cao, S. Li, H. Liu, G. Liu, and Y. Ma, Room-Temperature Superconductivity at 298 K in Ternary La-Sc-H System at High-pressure Conditions, arXiv:2510.01273 (2025).
- [8] M. Einaga, M. Sakata, T. Ishikawa, K. Shimizu, M. I. Eremets, A. P. Drozdov, I. A. Troyan, N. Hirao, and Y. Ohishi, Crystal structure of the superconducting phase of sulfur hydride, Nat. phys. 12, 835 (2016).
- [9] F. Du, A. P. Drozdov, V. S. Minkov, F. F. Balakirev, P. Kong, G. A. Smith, J. Yan, B. Shen, P. Gegenwart, and M. I. Eremets, Superconducting gap of H₃S measured by tunnelling spectroscopy, Nature 641, 619–624 (2025).
- [10] D. Duan, Y. Liu, F. Tian, D. Li, X. Huang, Z. Zhao, H. Yu, B. Liu, W. Tian, and T. Cui, Pressure-induced metallization of dense (H₂S)₂H₂ with high-T_c superconductivity, Sci. Rep. 4, 6968 (2014).
- [11] H. Wang, J. S. Tse, K. Tanaka, T. Iitaka, and Y. Ma, Superconductive sodalite-like clathrate calcium hydride at high pressures, Proc. Natl. Acad. Sci. 109, 6463 (2012).
- [12] I. Errea, M. Calandra, C. J. Pickard, J. Nelson, R. J. Needs, Y. Li, H. Liu, Y. Zhang, Y. Ma, and F. Mauri, High-pressure hydrogen sulfide from first principles: A strongly anharmonic phonon-mediated superconductor, Phys. Rev. Lett. 114, 157004 (2015).
- [13] H. Liu, I. I. Naumov, R. Hoffmann, N. Ashcroft, and R. J. Hemley, Potential high-T_c superconducting lan-

- thanum and yttrium hydrides at high pressure, Proc. Natl. Acad.Sci. 114, 6990 (2017).
- [14] F. Peng, Y. Sun, C. J. Pickard, R. J. Needs, Q. Wu, and Y. Ma, Hydrogen Clathrate Structures in Rare Earth Hydrides at High Pressures: Possible Route to Room-Temperature Superconductivity, Phys. Rev. Lett. 119, 107001 (2017).
- [15] C. J. Pickard, I. Errea, and M. I. Eremets, Superconducting hydrides under pressure, Annu. Rev. Condens. Matter Phys. 11, 57 (2020).
- [16] S. Di Cataldo, C. Heil, W. von der Linden, and L. Boeri, LaBH₈: Towards high- T_c low-pressure superconductivity in ternary superhydrides, Phys. Rev. B **104**, L020511 (2021).
- [17] K. P. Hilleke and E. Zurek, Tuning chemical precompression: Theoretical design and crystal chemistry of novel hydrides in the quest for warm and light superconductivity at ambient pressures, J. Appl. Phys. 131, 070901 (2022).
- [18] X.-L. He, W. Zhao, Y. Xie, A. Hermann, R. J. Hemley, H. Liu, and Y. Ma, Predicted hot superconductivity in LaSc₂H₂₄ under pressure, Proc. Natl. Acad. Sci. 121, e2401840121 (2024).
- [19] R. Lucrezi, P. P. Ferreira, S. Hajinazar, H. Mori, H. Paudyal, E. R. Margine, and C. Heil, Full-bandwidth anisotropic Migdal-Eliashberg theory and its application to superhydrides, Commun. Phys. 7, 33 (2024).
- [20] C. Renskers, C. D. Spataru, M. Zacharias, S. Duwal, T. Elmslie, P. A. Sharma, and E. R. Margine, Prediction of high-temperature superconductivity in LaH4 at low pressures, J. Mater. Chem. C 13, 20571 (2025).
- [21] N. W. Ashcroft, Metallic Hydrogen: A High-Temperature Superconductor?, Phys. Rev. Lett. 21, 1748 (1968).
- [22] J. Bardeen, L. N. Cooper, and J. R. Schrieffer, Theory of superconductivity, Phys. Rev. 108, 1175 (1957).
- [23] N. W. Ashcroft, Hydrogen Dominant Metallic Alloys: High Temperature Superconductors?, Phys. Rev. Lett. 92, 187002 (2004).
- [24] E. F. Talantsev, Classifying superconductivity in compressed H₃S, Mod. Phys. Lett. B 33, 1950195 (2019).
- [25] L. P. Gor'kov and V. Z. Kresin, Colloquium: High pressure and road to room temperature superconductivity, Rev. Mod. Phys. 90, 011001 (2018).
- [26] A. B. Migdal, Interaction between electrons and lattice vibrations in a normal metal, Sov. Phys. JETP 7, 996 (1958).
- [27] T. Jarlborg and A. Bianconi, Breakdown of the Migdal approximation at Lifshitz transitions with giant zeropoint motion in the H₃S superconductor, Sci. Rep. 6, 24816 (2016).
- [28] W. Sano, T. Koretsune, T. Tadano, R. Akashi, and R. Arita, Effect of Van Hove singularities on high-T_c superconductivity in H₃S, Phys. Rev. B 93, 094525 (2016).
- [29] S. B. Mishra, H. Mori, and E. R. Margine, Electronphonon vertex correction effect in superconducting H₃S, arXiv:2507.01897 (2025).
- [30] I. Errea, M. Calandra, C. J. Pickard, J. R. Nelson, R. J. Needs, Y. Li, H. Liu, Y. Zhang, Y. Ma, and F. Mauri, Quantum hydrogen-bond symmetrization in the superconducting hydrogen sulfide system, Nature 532, 81 (2016).
- [31] A. F. Goncharov, S. S. Lobanov, V. B. Prakapenka, and E. Greenberg, Stable high-pressure phases in the H-S sys-

- tem determined by chemically reacting hydrogen and sulfur, Phys. Rev. B **95**, 140101 (2017).
- [32] V. S. Minkov, V. B. Prakapenka, E. Greenberg, and M. I. Eremets, A Boosted Critical Temperature of 166 K in Superconducting D3S Synthesized from Elemental Sulfur and Hydrogen, Angew. Chem. Int. Ed 59, 18970 (2020).
- [33] M. Zacharias and F. Giustino, Theory of the special displacement method for electronic structure calculations at finite temperature, Phys. Rev. Res. 2 (2020).
- [34] H. Lee, S. Poncé, K. Bushick, S. Hajinazar, J. Lafuente-Bartolome, J. Leveillee, C. Lian, J.-M. Lihm, F. Macheda, H. Mori, H. Paudyal, W. H. Sio, S. Tiwari, M. Zacharias, X. Zhang, N. Bonini, E. Kioupakis, E. R. Margine, and F. Giustino, Electron-phonon physics from first principles using the EPW code, npj Comput. Mater. 9, 2057 (2023).
- [35] J. A. Flores-Livas, A. Sanna, and E. Gross, High temperature superconductivity in sulfur and selenium hydrides at high pressure, Eur. Phys. J. B 89, 1 (2016).
- [36] S. Mozaffari, D. Sun, V. S. Minkov, A. P. Drozdov, D. Knyazev, J. B. Betts, M. Einaga, K. Shimizu, M. I. Eremets, L. Balicas, et al., Superconducting phase diagram of H₃S under high magnetic fields, Nat. Commun. 10, 2522 (2019).
- [37] H. Nakao, M. Einaga, M. Sakata, M. Kitagaki, K. Shimizu, S. Kawaguchi, N. Hirao, and Y. Ohishi, Superconductivity of pure H₃S synthesized from elemental sulfur and hydrogen, J. Phys. Soc. Jpn. 88, 123701 (2019).
- [38] M. Eremets and A. P. Drozdov, High-temperature conventional superconductivity, Phys.-Usp. 59, 1154 (2016).
- [39] See the Supplemental Material for additional information. Figure S1 shows the superconducting gap of H₃S and D₃S at 200 GPa, computed using the FSR and FBW approaches with harmonic phonons, both with and without vertex corrections. Table S1 summarizes the superconducting properties of H₃S and D₃S computed in this study.
- [40] R. Szczeşńiak and A. Durajski, The isotope effect in H3S superconductor, Solid State Comm. 249, 30 (2017).
- [41] A. Durajski, R. Szczesńiak, and L. Pietronero, Hightemperature study of superconducting hydrogen and deuterium sulfide, Annalen der Physik 528, 358 (2016).
- [42] M. Komelj and H. Krakauer, Electron-phonon coupling and exchange-correlation effects in superconducting H₃S under high pressure, Phys. Rev. B 92, 205125 (2015).
- [43] P. Giannozzi, O. Andreussi, T. Brumme, O. Bunau, M. Buongiorno Nardelli, M. Calandra, R. Car, C. Cavazzoni, D. Ceresoli, M. Cococcioni, N. Colonna, I. Carnimeo, A. Dal Corso, S. de Gironcoli, P. Delugas, R. A. DiStasio Jr, A. Ferretti, A. Floris, G. Fratesi, G. Fugallo, R. Gebauer, U. Gerstmann, F. Giustino, T. Gorni, J. Jia, M. Kawamura, H. Y. Ko, A. Kokalj, E. Küçükbenli, M. Lazzeri, M. Marsili, N. Marzari, F. Mauri, N. L. Nguyen, H.-V. Nguyen, A. Otero-de-la Roza, L. Paulatto, S. Poncé, D. Rocca, R. Sabatini, B. Santra, M. Schlipf, A. P. Seitsonen, A. Smogunov, I. Timrov, T. Thonhauser, P. Umari, N. Vast, X. Wu, and S. Baroni, Advanced capabilities for materials modelling with Quantum ESPRESSO, J. Phys.: Condens. Matter 29, 465901 (2017).
- [44] D. R. Hamann, Optimized norm-conserving Vanderbilt pseudopotentials, Phys. Rev. B 88, 085117 (2013).
- [45] J. P. Perdew, K. Burke, and M. Ernzerhof, Generalized

- gradient approximation made simple, Phys. Rev. Lett. **77**, 3865 (1996).
- [46] M. Methfessel and A. T. Paxton, High-precision sampling for Brillouin-zone integration in metals, Phys. Rev. B 40, 3616 (1989).
- [47] S. Baroni, S. de Gironcoli, A. Dal Corso, and P. Giannozzi, Phonons and related crystal properties from density-functional perturbation theory, Rev. Mod. Phys. 73, 515 (2001).
- [48] F. Giustino, M. L. Cohen, and S. G. Louie, Electronphonon interaction using Wannier functions, Phys. Rev. B 76, 165108 (2007).
- [49] S. Poncé, E. Margine, C. Verdi, and F. Giustino, EPW: Electron-phonon coupling, transport and superconducting properties using maximally localized Wannier functions, Comput. Phys. Commun. 209, 116 (2016).
- [50] E. R. Margine and F. Giustino, Anisotropic Migdal-Eliashberg theory using Wannier functions, Phys. Rev.

- B 87, 024505 (2013).
- [51] N. Marzari, A. A. Mostofi, J. R. Yates, I. Souza, and D. Vanderbilt, Maximally localized Wannier functions: Theory and applications, Rev. Mod. Phys. 84, 1419 (2012).
- [52] G. Pizzi, V. Vitale, R. Arita, S. Blügel, F. Freimuth, G. Géranton, M. Gibertini, D. Gresch, C. Johnson, T. Koretsune, J. Ibañez-Azpiroz, H. Lee, J.-M. Lihm, D. Marchand, A. Marrazzo, Y. Mokrousov, J. I. Mustafa, Y. Nohara, Y. Nomura, L. Paulatto, S. Poncé, T. Ponweiser, J. Qiao, F. Thöle, S. S. Tsirkin, M. Wierzbowska, N. Marzari, D. Vanderbilt, I. Souza, A. A. Mostofi, and J. R. Yates, Wannier90 as a community code: new features and applications, J. Phys. Condens. Matter 32, 165902 (2020).
- [53] A. Marrazzo, S. Beck, E. R. Margine, N. Marzari, A. A. Mostofi, J. Qiao, I. Souza, S. S. Tsirkin, J. R. Yates, and G. Pizzi, Wannier-function software ecosystem for materials simulations, Rev. Mod. Phys. 96, 045008 (2024).

$\label{eq:Supplementary Information:} Supplementary Information: \\ Nonadiabatic and anharmonic effects in high-pressure H_3S and D_3S superconductors$

Shashi B. Mishra^{1,*} and Elena R. Margine^{1,†}

¹Department of Physics, Applied Physics and Astronomy,
Binghamton University-SUNY, Binghamton, New York 13902, USA

(Dated: October 31, 2025)

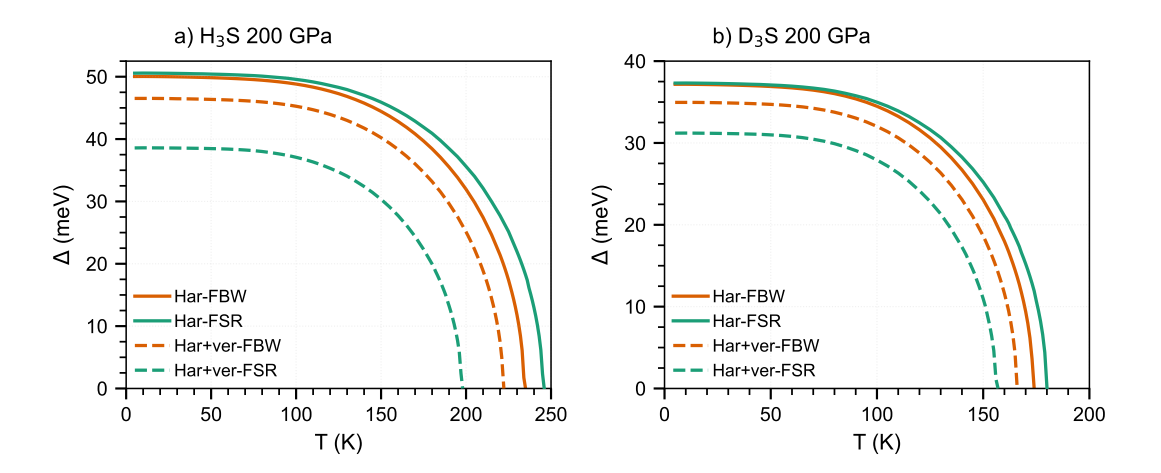


Figure. S1. Isotropic superconducting gap $\Delta(T)$ calculated for a) H₃S and b) D₃S at 200 GPa using harmonic phonons and an effective Coulomb pseudopotential $\mu_{\rm E}^*=0.16$. Results are shown for four approaches: FBW (orange), FSR (teal-green), vertex-corrected FBW (dashed orange), and vertex-corrected FSR (dashed teal-green).

TABLE S1. Zero-temperature superconducting gap $\Delta(0)$, critical temperature T_c , and isotope coefficient $\alpha = -\ln(T_c^{\mathrm{D_3S}} - T_c^{\mathrm{H_3S}})/\ln(M^{\mathrm{D_3S}} - M^{\mathrm{H_3S}})$ obtained from the FSR and FBW approaches, with and without vertex corrections for H₃S and D₃S, incorporating anharmonic phonons at 160 GPa and both harmonic and anharmonic phonons at 200 GPa. All superconductivity calculations employ a Coulomb pseudopotential $\mu_{\rm E}^*$ =0.16. Experimental α values are taken from Ref. [1–3].

Material	Pressure (GPa)	Phonons	Method	$\Delta(0) \; (\text{meV})$	$T_{\rm c}$ (K)	α	α^{Exp}	
$ m H_3S$		Anh	FSR	39.69	205	0.37		
	160		FBW	44.94	219	0.38	0.22 – 0.34	
	100	11111	ver-FSR	36.49	191	0.34		
			$ver ext{-}FBW$	43.49	213	0.37		
			FSR	50.55	246	0.45		
		Har	FBW	50.03	235	0.44	0.23-0.38	
			ver-FSR	38.56	198	0.34		
	200		$ver ext{-}FBW$	46.52	222	0.42		
		Anh	FSR	36.41	192	0.34		
			FBW	37.07	189	0.33		
			ver-FSR	28.84	157	0.25		
			$ver ext{-}FBW$	34.51	178	0.32		
$\mathrm{D_{3}S}$		Anh	FSR	31.32	159			
	160		FBW	35.05	168			
			ver-FSR	29.53	151			
			$ver ext{-}FBW$	34.09	165			
			FSR	37.31	180			
		Har	FBW	37.17	174			
			ver-FSR	31.19	157			
	200		$ver ext{-}FBW$	34.96	166			
			FSR	29.40	152			
		Anh	FBW	29.81	150			
			ver-FSR	24.78	132			
			$ver ext{-}FBW$	28.08	143			

^{*} mshashi125@gmail.com

[†] rmargine@binghamton.edu

^[1] A. P. Drozdov, M. I. Eremets, I. A. Troyan, V. Ksenofontov, and S. I. Shylin, Nature 525, 73 (2015).

^[2] V. S. Minkov, V. B. Prakapenka, E. Greenberg, and M. I. Eremets, Angew. Chem. Int. Ed 59, 18970 (2020).
[3] F. Du, A. P. Drozdov, V. S. Minkov, F. F. Balakirev, P. Kong, G. A. Smith, J. Yan, B. Shen, P. Gegenwart, and M. I. Eremets, Nature 641, 619-624 (2025).